Self-assembled tetrahedral framework nucleic acid mediates tumor-associated macrophage reprogramming and restores antitumor immunity

Husun Qian,[1,4] Ting Zhou,[1,4] Yixin Fu,[1] Minkang Guo,[2] Wu Yang,[2] Dian Zhang,[1] Wenli Fang,[1] Mengli Yao,[1] He Shi,[1] Chengsen Chai,[1] Wei Cheng,[3] Shijia Ding,[1] and Tingmei Chen[1]

[1]Key Laboratory of Clinical Laboratory Diagnostics (Ministry of Education), College of Laboratory Medicine, Chongqing Medical University, Chongqing 400016, P.R. China; [2]Department of Orthopedics, The First Affiliated Hospital of Chongqing Medical University, Chongqing 400016, China; [3]The Center for Clinical Molecular Medical Detection, The First Affiliated Hospital of Chongqing Medical University, Chongqing 400016, China

There is increasing interest in depleting or repolarizing tumor-associated macrophages (TAMs) to generate a proinflammatory effect. However, TAMs usually display an immunosuppressive M2-like phenotype in the tumor microenvironment. Apparently, developing a macrophage-targeting delivery system with immunomodulatory agents is urgent. In this study, an efficient siRNA and CpG ODNs delivery system (CpG-siRNA-tFNA) was prepared with nucleic acid stepwise self-assembled. The tFNA composed of CpG ODNs and siRNA showed a higher stability and an enhanced cellular uptake efficiency. Moreover, the CpG-siRNA-tFNA effectively reprogrammed TAMs toward M1 phenotype polarization with increased proinflammatory cytokine secretion and NF-κB signal pathway activation, which triggers dramatic antitumor immune responses. Additionally, the CpG-siRNA-tFNA exhibited superior antitumor efficacy in a breast cancer xenograft mouse model without obvious systemic side effects. Taken together, CpG-siRNA-tFNA displayed greatly antitumor effect by facilitating TAM polarization toward M1 phenotypes in favor of immunotherapy. Hence, we have developed an efficient therapeutic strategy with immunomodulatory agents for clinical applications.

INTRODUCTION

Tumor-associated macrophages (TAMs) are mainly derived from monocytes in the blood circulation and tissue-resident macrophages, which constitute up to 50% of cell populations in tumor mass.[1,2] As an important component of tumor microenvironment (TME), TAMs play a key role in tumor growth, invasion, and metastasis.[3,4] According to different activation manners, TAMs are divided into a classically activated M1 phenotype and an alternatively activated M2 phenotype.[5] Most studies have shown that M1 macrophages initiate proinflammatory cytokine production and activate immune response and tumoricidal activity.[6,7] Conversely, M2 macrophages secrete anti-inflammatory cytokine, suppress adaptive immunity, and facilitate tumor growth and progression.[8,9] Of note, TAMs usually display an immunosuppressive M2-like phenotype under the influence of the TME, such as hypoxia and acidity pH.[10–12] In addition, clinical

studies have further shown that the presence of TAMs in TME is related to a poor prognosis in a variety of human cancers.[13–15] Thus, it is a potential therapeutic strategy to reprogram TAMs toward antitumoral M1 macrophage polarization for tumor eradication.

In recent years, TAMs have emerged as an attractive potential therapeutic target for cancer immunotherapy. So far, a variety of immune-modulator-mediated TAMs-M1 reprogramming have been applied to restore the antitumoral immunity, such as microRNA, cytosine-guanosine oligodeoxynucleotides (CpG ODNs), small interfering RNA (siRNA), antisense oligodeoxynucleotide (ASO), and small-molecule inhibitor.[16–21] Among these, siRNA is a powerful molecular tool to knock down specific gene expression in the field of gene therapy. It interferes with the expression of specific genes with complementary nucleotide sequences by degrading mRNA after transcription within the RNA interference pathway.[22–24] However, there are some drawbacks to hinder this free form of siRNA therapeutic efficiency, including low efficiency of cellular uptake, poor stability, and short period of action.[25,26] Apparently, developing a delivery system that can effectively overcome these challenges and specifically deliver siRNA to TAMs is urgent.

DNA framework nucleic acid (FNA) is an emerging field of DNA-based nanotechnology with controllable size and shape, including DNA origami, tetrahedra, triangle, Y-shape, and so on.[27,28] Moreover, many studies reported that self-assembled DNA FNA can efficiently deliver various immune modulators into cells due to its inherent biocompatibility, high biosecurity, and low cost. For example, Zhang et al. developed a DNA tetrahedron-based nanogel based on a cross-linking strategy for intracellular EGFR siRNA delivery, which can
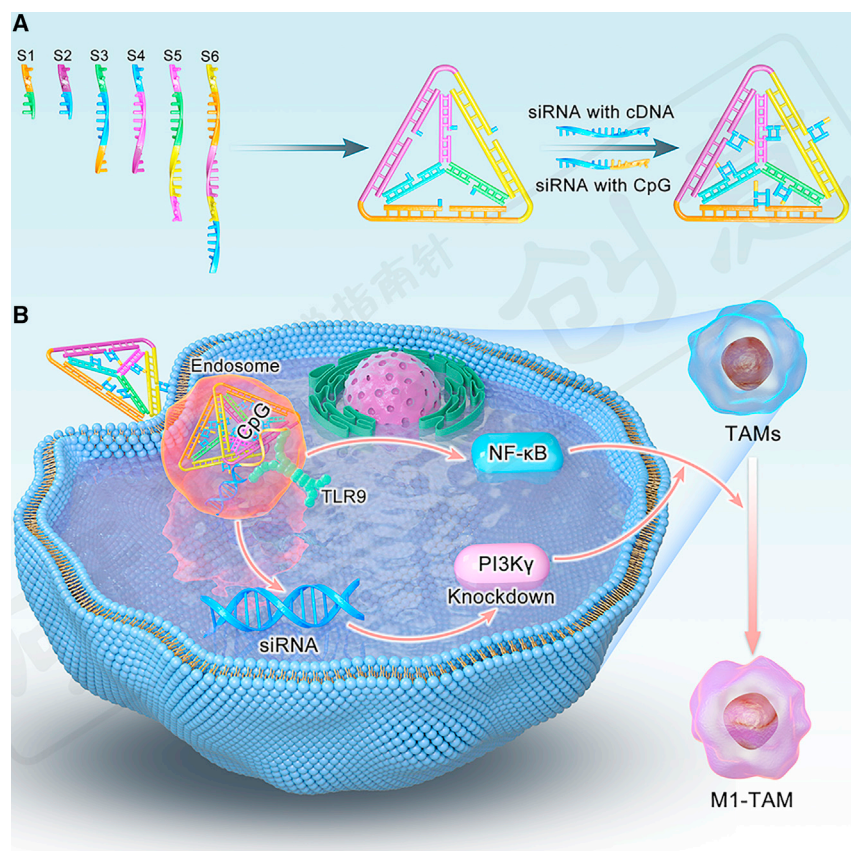
Figure 1. System design and immunotherapeutic effects of CpG-siRNA-tFNA

(A) Schematic illustration of DNA strands for CpG-siRNA-tFNA formation (each color corresponds to one of the six edges of the tFNA). (B) Delivery of CpG ODNs and siRNA for inducing immunostimulation and reprogramming in TAMs.

known, CpG ODNs could be efficiently internalized by macrophages with Toll-like receptor 9 (TLR9)-dependent activation.[33] The binding of TLR9 and CpG ODNs can trigger innate and adaptive immune responses.[34] As an immunostimulatory TLR9 agonist, CpG ODNs are already in preclinical studies for melanoma.[35] Likewise, the design of CpG-siRNA-tFNA utilizes a Dicer-substrate 25/27-mer siRNA sequence to enable cleavage of the CpG-siRNA-tFNA, releasing 21-mer siRNA from the receptor-bound CpG fragment. Then, diced siRNA molecules are translocated from endosomes to ER where they can interact with the RNA interference machinery.[36,37]

Meanwhile, it is reported that phosphatidylinositol 3-kinase-γ (PI3Kγ) acts as a molecular switch turning on immunosuppression while shutting down immune-stimulatory activities in TAMs.[38] In particular, most studies have shown that PI3Kγ inhibition facilitates M2-like TAMs toward M1 phenotype polarization.[39,40] Additionally, PI3Kγ also restrains TLRs-mediated inflammation and signaling pathway activation.[41,42] We hypothesize that simultaneously inhibiting PI3Kγ and activating TLRs could effectively reprogram TAMs toward a more proinflammatory phenotype and inhibit tumor progression. As shown in Figure 1B, the binding of CpG ODNs and TLR9 facilitated the uptake of the siRNA component into the cytosol for efficient gene silencing. As such, PI3Kγ inhibition effectively enhanced CpG ODN's activation function for the NF-κB signaling pathway. Finally, the combination of CpG ODN immunostimulation and PI3Kγ expression downregulation would effectively reprogram TAMs toward M1 phenotype polarization and exhibit a potent anticancer efficacy.

efficiently enter the cells and downregulate the EGFR gene expression.[29] Ding et al. fabricated a versatile triangular DNA origami to co-deliver siRNA and chemo-drugs into target cells for an enhanced synergistic antitumor effect.[30] Shi et al. reported a novel spherical nucleic acid conjugate with superior biocompatibility for siRNA delivery, which showed potent gene knockdown at both mRNA and protein levels.[31] Sleiman et al. designed a flexible DNA "nanosuitcase" for siRNA-encapsulating and release in live cells on demand.[32] These self-assembled DNA FNA could effectively deliver additional therapeutic components into cells with improved dispersibility and stability, and thus enhance the therapeutic efficacy.

Here, we explored a facile strategy of linking siRNAs and CpG ODNs to a tetrahedral framework nucleic acid (tFNA) to combine delivery to TAM cells. As shown in Figure 1A, six DNA strands with complementary overhangs at the 3′ ends can self-assemble into a tFNA, which is different from traditional DNA tetrahedralbased four-DNA-strand assembly. We designed the tFNA to contain a nick in the middle position of each edge. The overhang at this nick is complementary to the siRNA (AS)-overhang strands. Moreover, the siRNA (SS)-CpG strands are also integrated into the tFNA by complementary base-pairing of the sense strand and antisense strand of the siRNA. Specifically, the tFNA with controllable loading density can simultaneously deliver siRNAs and CpG ODNs into cells. As is well
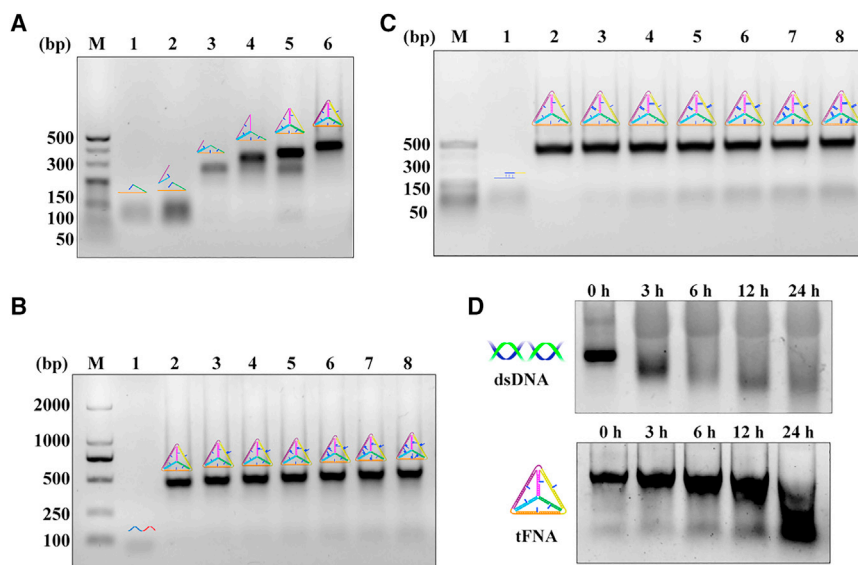
RESULTS

Preparation and characterization of CpG-siRNA-tFNA

CpG-siRNA-tFNA could be readily prepared using the designed strand (Table S1), and the self-assembled process is presented in Figure 1A. In order to demonstrate the stepwise assembly procedure, we separately constructed tFNA, CpG-tFNA, and CpG-siRNA-tFNA. The successful preparation of nucleic acid nanostructures was confirmed by gel electrophoresis. As showed in Figure 2A, a distinct band shift was observed along with different strands introduced, indicating tFNA assembly nanostructure formation. For different valence numbers CpG-tFNA nanostructure formation, CpG-overhang

Figure 2. Preparation and characterization of CpG-siRNA-tFNA

(A) Agarose gel electrophoresis analysis to confirm self-assembly of the tFNA (Lane 1, S1. Lane 2, S1 + S2. Lane 3, S1 + S2 + S3. Lane 4, S1 + S2 + S3 + S4. Lane 5, S1 + S2 + S3 + S4 + S5. Lane 6, S1 + S2 + S3 + S4 + S5 + S6, tFNA). (B) Agarose gel electrophoresis analysis to confirm the hybridization of CpG ODNs to the tFNA (Lane 1, CpG-overhang. Lane 2, tFNA. Lane 3, tFNA with 1 CpG. Lane 4, tFNA with 2 CpG. Lane 5, tFNA with 3 CpG. Lane 6, tFNA with 4 CpG. Lane 7, tFNA with 5 CpG. Lane 8, tFNA with 6 CpG). (C) Agarose gel electrophoresis analysis to confirm the hybridization of siRNA to the tFNA (Lane 1, CpG-overhang. Lane 2, tFNA. Lane 3, tFNA with 1 siRNA. Lane 4, tFNA with 2 siRNA. Lane 5, tFNA with 3 siRNA. Lane 6, tFNA with 4 siRNA. Lane 7, tFNA with 5 siRNA. Lane 8, tFNA with 6 siRNA). (D) Electrophoresis analysis of the stability of tFNA.

strands were added together in different proportions. The gel electrophoresis analysis results are shown in Figure 2B. The band mobility slightly decreased with the increase of CpG-overhang strand number, which was attributed to slight differences in each nanostructure's molecular weight. Similarly, different valence numbers of CpG-siRNA-tFNA were constructed and analyzed by gel electrophoresis. As shown in Figure 2C, the band's mild movement was observed with the increase of the siRNA (SS)-CpG strand and siRNA (AS)-overhang strand number. The results suggested that these functional nucleic acid nanostructures were successfully synthesized. Moreover, it showed that CpG and siRNA could be modified to tFNA with controllable density. Also, The CpG-siRNA-tFNA structure was imaged by atomic force microscopy (AFM); the results are shown in Figure S1.

Since DNA tFNA was reported to effectively resist nuclease degradation,[43] we investigated the stability of tFNA in 10% non-inactivated fetal bovine serum. We compared the stability of dsDNA and tFNA at 37°C for different time periods. As shown in Figure 2D, the band of dsDNA almost disappeared with 3 h of incubation. On the other hand, the band of tFNA remained nearly unchanged after 3 h of incubation. However, we observed that the band of tFNA gradually moved down and diffused with the incubation time extended, especially after 24 h. The phenomenon reflected that the tFNA nanostructure suffered partial degradation. Nevertheless, there was still a strong band of tFNA after 24 h of incubation; therefore, the tFNA could resist nuclease degradation and possessed a higher stability than the dsDNA in the fetal bovine serum.

Cell uptake and cytotoxicity of DNA tetrahedral nanostructures

Cellular uptake efficiency of DNA tetrahedral nanostructures was investigated with a fluorescently labeled CpG strand. Confocal imaging showed that the CpG-tFNA group presented intense FAM fluorescence in the cytoplasm (Figure 3A). In contrast, the CpG control group showed negligible fluorescence. The results suggested that the tFNA nanostructure was more readily taken up by cells, which might be also related to the higher stability of tFNA and the ability of tFNA in driving the nanostructures into cells. Besides, the endosomal location of the CpG-binding TLR9 is advantageous for facilitating the siRNA component to reach the cytosol for efficient gene silencing. In order to verify this concept, RAW 264.7 cells were incubated with siRNA-tFNA or CpG-siRNA-tFNA for 1 h. Confocal imaging showed that the CpG-siRNA-tFNA group presented intense fluorescence intensity compared with the siRNA-tFNA group (Figure S2).

The viability of RAW 264.7 cells exposed to different concentrations of CpG-tFNA and CpG-siRNA-tFNA were evaluated with a standard CCK-8 assay. As shown in Figure 3B, there were no measurable effects on cells' metabolic activity and CpG-tFNA and CpG-siRNA-tFNA even when both stimulated the growth of the cells. Moreover, CpG-tFNA and CpG-siRNA-tFNA both exhibited more significant stimulation efficiency along with increasing nanostructure concentration, which were attributed to the immunostimulatory activity of CpG motifs.

Immunostimulation effects of CpG-siRNA-tFNA

To evaluate the immunostimulatory activity of CpG-siRNA-tFNA, the secretion levels of proinflammatory cytokines (TNF-α, IL-6, and IL-12) in RAW 264.7 cells were measured by ELISA. As demonstrated in Figure 4, CpG-tFNA showed significantly increased immunostimulatory activity for the proinflammatory cytokine secretion compared with free CpG ODNs. The results were primarily attributed to the greatly enhanced stability and cellular uptake efficiency of CpG-tFNA. Moreover, the induction of proinflammatory cytokine level was further improved by increasing the number of CpG motifs per tFNA nanostructure. More importantly, CpG-siRNA-tFNA

A

B
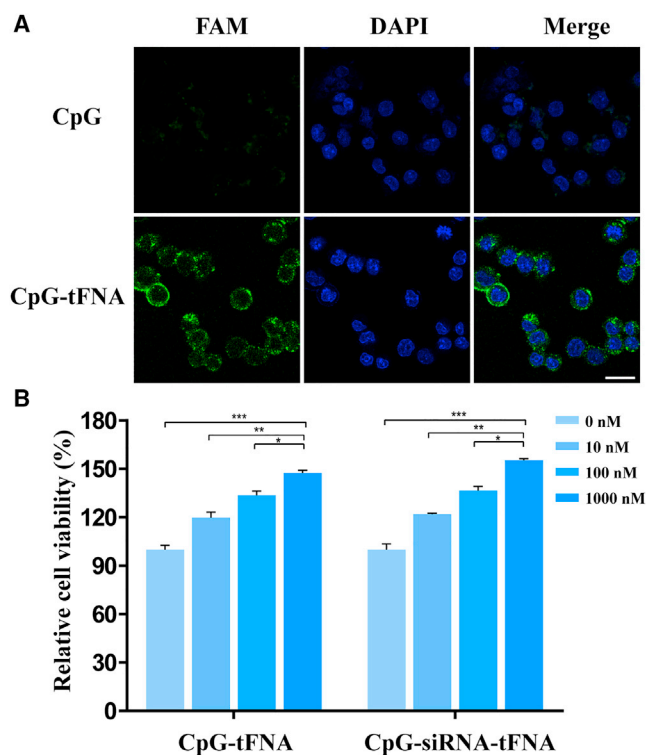
Figure 3. Cell uptake and cytotoxicity of DNA tetrahedral nanostructures
(A) Confocal laser scanning microscopy images analysis of the difference of cellular uptake between CpG and CpG-tFNA (scale bar = 20 μm). (B) Cell viability assay (CCK-8 assay) of RAW 264.7 cells after treatment with different concentrations of CpG-tFNA and CpG-siRNA-tFNA for 24 h. The error bars are standard deviations of measurements repeated three times. Statistical analysis was performed using ANOVA with multiple comparisons. For all panels, *p < 0.05, **p < 0.01, ***p < 0.001, ****p < 0.0001.

showed much stronger immunostimulatory capability, which induced dramatically higher amounts of the cytokine secretion. To prove that silencing PI3Kγ enhances the CpG ODN-mediated immunostimulatory effect, we compared the immunostimulatory activity of 6CpG-control siRNA-tFNA and 6CpG-PI3Kγ-siRNA-tFNA (Figure S3). The results indicated that the proinflammatory cytokine secretion was synergistically triggered by both CpG ODN stimulation and PI3Kγ inhibition. These results also show that the tFNA nanostructures possess special superiority that can simultaneously carry siRNAs and CpG ODNs with high loading density. As such, the qPCR results of the proinflammatory cytokine levels were consistent with the ELISA results (Figure S4).

Macrophage polarization by immunostimulatory CpG-siRNA-tFNA

To validate the macrophage polarization markers, RAW 264.7 were treated with LPS and IL-4 for 24 h, respectively. The Western blot results (Figure S5B) confirmed the expression of M1 marker (inducible nitric oxide synthase [iNOS]) and M2 marker (arginase-1 [Arg-1]). In

addition, we observed the morphological changes in different types polarization of macrophages (Figure S5A).

As is well known, enhanced secretion of proinflammatory cytokines is a major characteristic of M1-phenotype macrophages. And NF-κB is a major signal pathway participating in the expression of a variety of cytokines after the stimulation of CpG-siRNA-tFNA. Therefore, we investigated the macrophage phenotype transformation and NF-κB signal pathway activation. As shown in Figure 5A, CpG-siRNA-tFNA induced iNOS expression and stimulated NF-κB p65 subunit phosphorylation in RAW 264.7 cells. More importantly, PI3Kγ inhibition increased CpG-inducible iNOS expression and CpG-stimulated phosphorylated p65 expression levels.
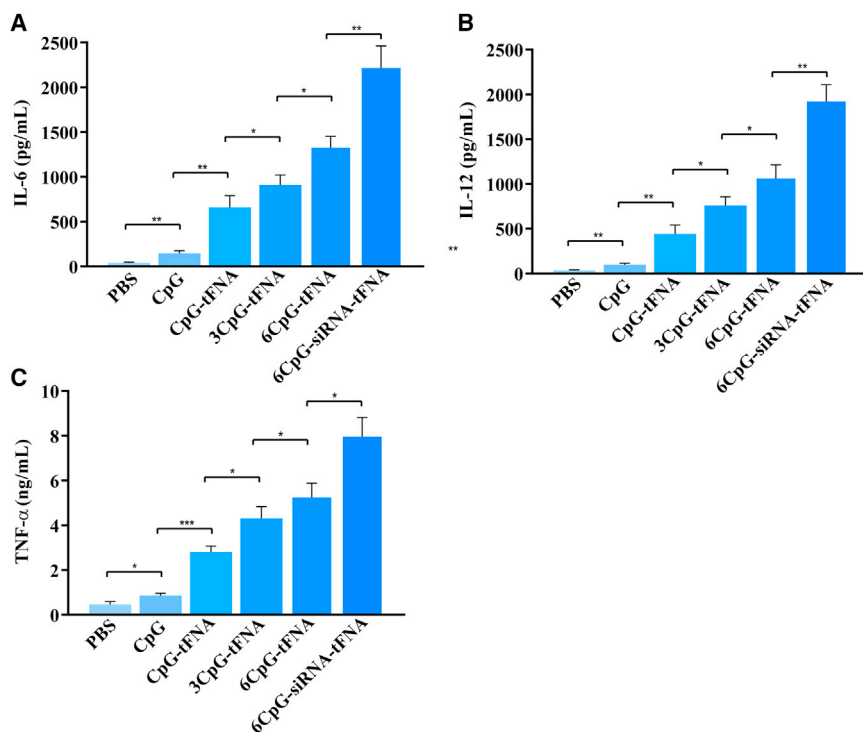
Subsequently, we investigated whether PI3Kγ expression downregulation promoted M2 macrophages toward M1 phenotype polarization. Macrophages were first induced toward M2 phenotype polarization upon stimulation with IL-4. Consistent with previous studies, IL-4 induced a remarkable Arg-1 expression (Figure 5B), whereas PI3Kγ knockdown evidently inhibited Arg-1 expression and enhanced CpG-stimulated iNOS expression. Furthermore, we examined the macrophages' phenotype switch based on characteristic expression profiles of surface markers by flow cytometry. As detected by flow cytometry, Figures 5C and 4D show a dramatic increase in CD86 expression (a M1 marker) and very slight increases in CD206 expression (a M2 marker) with CpG stimulation. In accord with previous results, PI3Kγ knockdown enhanced CpG-stimulated CD86 expression and reduced CD206 expression. These results demonstrated that PI3Kγ inhibition effectively reprogrammed TAMs toward M1 phenotype polarization and enhanced CpG ODN's activation function for the NF-κB signaling pathway in macrophages.

Furthermore, we extracted BALB/c mice bone marrow-derived macrophages for polarization assays. As shown in Figure S6, CpG-tFNA-induced iNOS expression and PI3Kγ inhibition increased CpG-inducible iNOS expression, which were consistent with RAW 264.7 cells.

Antitumor effects of CpG-siRNA-tFNA *in vitro*

In the current study, we chose 4T1 breast cells as typical tumorous cells to analyze antitumor activity of CpG-siRNA-tFNA-treated macrophages. As shown in Figure 6A, RAW 264.7 cells were cocultured with 4T1 cells in the transwell system. CpG-stimulated macrophages revealed obvious antiproliferative effects on 4T1 cells. More importantly, CpG-siRNA-tFNA-treated macrophages showed higher antiproliferative efficacy with PI3Kγ knockdown. Moreover, cellular viability of 4T1 cells declined rapidly with macrophage supernate concentration increasing (Figure 6B). These results taken together, PI3Kγ inhibition further stimulated higher amounts of immune cytokine secretion in macrophages, which strongly inhibited the proliferation of the 4T1 cells.

During this investigation, the activity of caspase-3 was also determined with the caspase-3 activity kit. In accord with previous results,

ulation, 4T1-bearing mice were randomly divided into three groups. Each group was respectively treated with PBS, CpG-tFNA, and CpG-siRNA-tFNA by tail vein injection every other day. Notably, CpG-siRNA-tFNA significantly suppressed tumor growth, and CpG-tFNA partly delayed tumor growth (Figure 7D). Most significantly, the CpG-siRNA-tFNA group displayed the most remarkable tumor growth inhibition efficacies and greatly prolonged the survival time of 4T1-bearing mice compared with the other control groups (Figures 7E and 6F).

To further confirm immunotherapeutic efficacy, tumor tissues from different groups were analyzed by immunohistochemical staining. Consistent with the tumor growth results, Ki-67-positive cells were significantly decreased in the CpG-siRNA-tFNA group (Figure S7). The results demonstrated that tumor cell proliferation was effectively inhibited. Moreover, immunofluorescence dual staining showed that the M1 phenotype marker (iNOS) was significantly up-regulated, whereas the M2 phenotype marker (Arg-1) was significantly down-regulated, in the CpG-siRNA-tFNA group compared with the control groups (Figure 7G). This phenomenon indicated that infiltrating macrophages shifted toward the M1 phenotypes.

Also, hematoxylin-eosin (H&E) staining showed more necrotic area with obvious nucleus shrinkage in the tumor tissue sections in the CpG-siRNA-tFNA group (Figure S8). Moreover, potential *in vivo* toxicity was studied by H&E staining of major organs. As shown in Figure S9, there was no appreciable pathological change observed in the different groups. Also, CpG-RNAi-tFNA treatment showed slightly increased cytokine secretion compared with the control group, which suggests that there was no systemic tissue damage or inflammation (Figure S10). These results taken together, CpG-siRNA-tFNA displayed a large antitumor effect by facilitating TAM polarization toward M1 phenotypes in favor of immunotherapy.

the activity of caspase-3 was significantly increased in the 4T1 cells incubated with macrophages together with CpG-tFNA or CpG-siRNA-tFNA (Figure 6C).

To further quantify apoptosis of tumor cells, we used flow cytometry to analyze the macrophage-mediated apoptosis after incubation with CpG-siRNA-tFNA for 24 h. Results showed that the apoptotic cell percentage obviously increased in CpG-tFNA and CpG-siRNA-tFNA groups compared with the control group (Figures 6D and 5E). Clearly, these results prove that CpG-siRNA-tFNA-treated macrophages effectively inhibit tumor cell proliferation and promote tumor cell apoptosis, which exhibit strong immunostimulatory and antitumor activity.

In vivo distribution of CpG-siRNA-tFNA
We next evaluated the *in vivo* distribution and stability of CpG-siRNA-tFNA. The results showed that the CY7-labeled CpG-siRNA-tFNA fluorescence intensity in tumor increased gradually until reaching the highest at 12 h (Figure 7B). At 48 h after tail vein injection, the tumor site showed very low fluorescence intensity, indicating an almost complete clearance. According to this result, the main organs and tumors were imaged at 12 h post-injection to examine the *in vivo* distribution of CpG-siRNA-tFNA. As shown in Figure 7C, the tumor, liver, and lung were major accumulated locations.

Immunotherapeutic effects of CpG-siRNA-tFNA *in vivo*
On the basis of the results above, we next explored immunotherapeutic effects of CpG-siRNA-tFNA *in vivo*. 4T1-bearing mice were treated according to the schedule in Figure 7A. On day 14 after the tumor inoc-

DISCUSSION
It is well known that TAMs are an important component of the TME, which play key functions in tumor growth, invasion, and metastasis. In this study, we fabricated an efficient siRNA and CpG ODN delivery system (CpG-siRNA-tFNA) based on nucleic acid stepwise self-
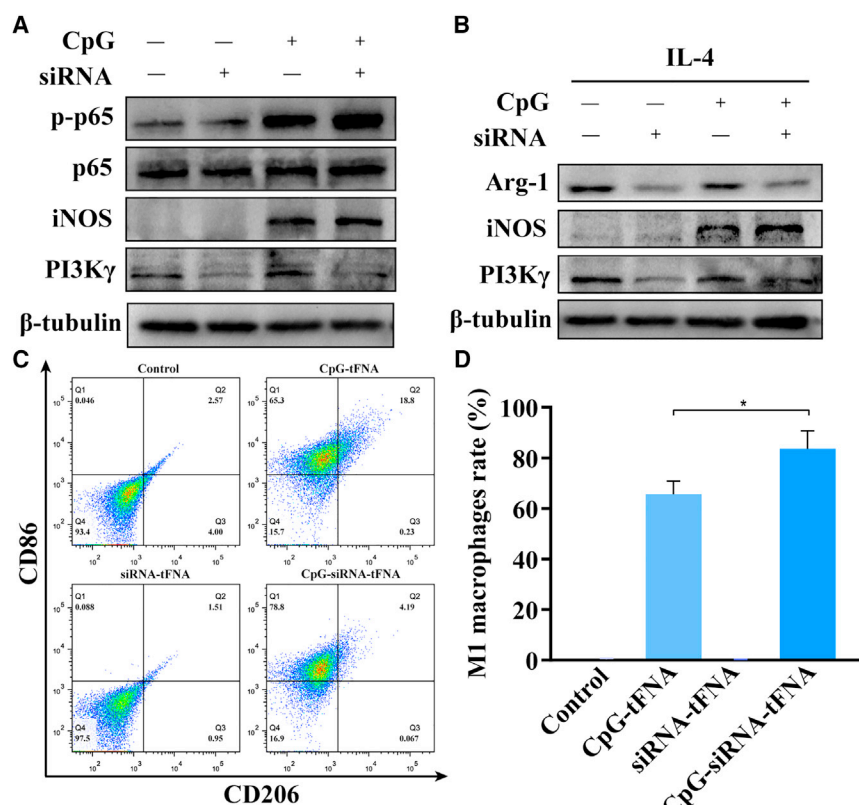
**Figure 5. Macrophage polarization by immunostimulatory CpG-siRNA-tFNA**

(A and B) Western blot analysis of protein expression involved in NF-κB signal pathways (A) and macrophages markers (B) in RAW 264.7 cells. (C) Flow cytometry analysis of the expression of CD86 and CD206 in RAW264.7 cells after treatment with different immunomodulatory agents for 24 h. (D) Statistical analysis of data. The error bars are standard deviations of measurements repeated three times. Statistical analysis was performed using ANOVA with multiple comparisons. For all panels, *p < 0.05, **p < 0.01, ***p < 0.001, ****p < 0.0001.

assembly with controllable loading density and high delivery efficiency. The system encompasses three activities in a single molecule: targeting moiety, TLR9 receptor activation, and gene silencing. Moreover, the CpG-siRNA-tFNA effectively reprograms TAMs toward M1 phenotype polarization with CpG ODNs immunostimulation and PI3Kγ expression downregulation. Furthermore, CpG-siRNA-tFNA induces macrophages to dramatically upregulate proinflammatory cytokines together with the activated NF-κB-signaling pathways, which triggers apparent antitumor immune responses for the effective inhibition of tumor cell proliferation. All together, our results indicate that the CpG-siRNA-tFNA is a favorable gene-silencing delivery vector.

Previous studies have shown that the transcription factor NF-κB is a key player in regulating the functions of macrophages.[44] CpG ODN interacts with TLR9, initiating a signaling cascade that proceeds through myeloid differentiation primary response gene 88 (MYD88) and culminates in the translocation of NF-κB. Then, the NF-κB p65 is activated and phosphorylated, which initiates p-p65 translocation into cell nuclei driving proinflammatory gene transcription. NF-κB activation skews the TAMs to an antitumoral M1 phenotype.[45,46] Furthermore, PI3Kγ expression downregulation promotes IκBα degradation and therefore enhances NF-κB-dependent production of inflammatory cytokines.[38] Consequently, antitumor immune responses are enhanced, coupled with PI3Kγ expression inhibition and CpG ODN immunostimulation.

Even so, the stability of CpG-siRNA-tFNA still needs to improve due to nuclease degradation under physiological conditions. In this study, we investigated the stability of tFNA in 10% non-inactivated fetal bovine serum, which showed that it could resist nuclease degradation and possessed a higher stability than dsDNA. Additionally, we further studied CpG-siRNA-tFNA application in vivo. Nevertheless, the consumption of oligonucleotides is enormous, which increases the therapeutic cost. Hence, a variety of metal nanoparticle-mediated TAMs-M1 reprogramming have been applied to restore the antitumoral immunity, such as ferumoxytol, MnO_2 nanoparticles, and $CaCO_3$ nanoparticles.[20,47,48] In general, these delivery system-based nanoparticles have higher stability compared with our proposed CpG-siRNA-tFNA under physiological conditions. Nevertheless, the delivery system-based nanoparticles frequently need complex synthesis steps, and the biocompatibility needs further improvement, which limit their further applications in biomedicine. Therefore, future research should focus on the rational design to comprehensively improve their stability and biocompatibility. In this respect, DNA framework-based hybrid nanomaterials is an effective approach to comprehensively enhance the performance of DNA frameworks and improve nanomaterial biocompatibility, such as hybrid DNA tetrahedral and hybrid DNA nanoflowers.[49,50] These rational designs utilize the advantages of DNA nanostructures, including intrinsic biocompatibility, programmable molecular recognition ability, and structural predictability. Meanwhile, metal nanoparticles provide protection from enzymatic degradation for nucleic acids, which become excellent candidates for enhancing the performance of DNA frameworks.

Besides, different nucleic acid modification techniques have been developed to protect DNA from nuclease degradation, such as 2′-F, 2′-NH2, or 2′-Ome substitutions.[51–53] Additionally, replacement of ribonucleotide analogs with locked nucleic acid (LNA) or threose nucleic acid (TNA) also exhibits superior resistance to nuclease-mediated digestion.[54–56] The application of modification to prevent nucleic acids from nuclease degradation is an effective strategy. All
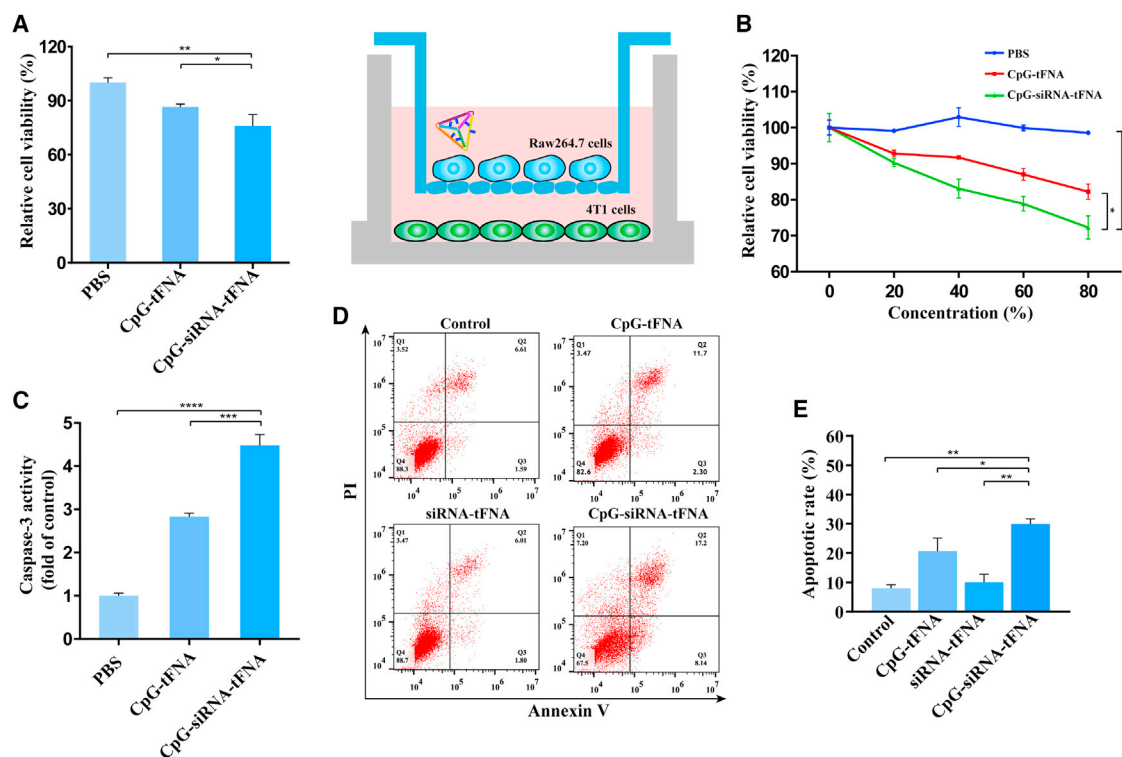
Figure 6. Antitumor effects of CpG-siRNA-tFNA *in vitro*

(A) RAW 264.7 cells were cocultured with 4T1 cells in the Transwell system and the cell viability was assessed by the CCK-8 assay. (B) 4T1 cells were incubated with different s of macrophage supernates, and cell viability was assessed by the CCK-8 assay. (C) The activity of 4T1 cell caspase-3 was determined *in vitro*. (D) Cell apoptosis was detected by flow cytometry at 24 h. (E) Statistical analysis of data. The error bars are standard deviations of three repetitive measurements. Statistical analysis was performed using ANOVA with multiple comparisons. For all panels, *p < 0.05, **p < 0.01, ***p < 0.001, ****p < 0.0001.

together, more studies are necessary to provide a rational basis for further development of the CpG-siRNA approach and improve CpG-siRNA gene-silencing effects for clinical applications.

## MATERIALS AND METHODS

Materials

All DNA oligonucleotide sequences were synthesized and purified by Sangon Biotechnology (Shanghai, China). siRNA (SS)-CpG and siRNA (AS)-Overhang were purchased from TaKaRa Biotechnology (Dalian, China). PI3Kγ siRNA were designed and synthesized by GenePharma (Shanghai, China). All oligonucleotide sequences are shown in Table S1. Antibody against PI3Kγ (cat no. sc-166365) was purchased from Santa Cruz Biotechnology (Santa Cruz, CA, USA). Antibodies for iNOS (cat no. 13120S), Arg-1 (cat no. 93668S), NF-κB p65 (cat no. 8242S), and phospho-NF-κB p65 (Ser536; cat no. 3033S) were obtained from Cell Signaling Technology (Danvers, MA, USA). Antibodies against β-tubulin (cat no. AP0064) were purchased from Bioworld Technology (Nanjing, China). The anti-CD16/32 (cat no. 101,301), anti-CD86 (cat no. 105,005), and anti-CD206 (cat no. 141,705) were obtained from BioLegend (San Diego, CA, USA). The horseradish peroxidase (HRP)-conjugated anti-rabbit IgG secondary antibodies (cat no. A0208) were purchased from Beyotime Biotechnology (Shanghai,

China). Mouse IL-1β ELISA Kit (cat no. 70-EK201B/3-96), Mouse IFN-γ ELISA Kit (cat no. 70-EK280/3-96), Mouse TNF-a ELISA Kit (cat no. 70-EK282/4-96), Mouse IL-12p70 ELISA Kit (cat no. 70-EK212/3-96) and Mouse IL-6 ELISA Kit (cat no. 70-EK206/3-96) ELISA kits were obtained from MultiSciences Biotechnology (Hangzhou, China). Total RNA extraction kit (cat no. Z3101) was obtained from Promega (Madison, WI, USA). The caspase-3 activity kit (cat no. C1115) and Annexin V–FITC/PI Apoptosis Detection Kit (cat no. C1062M) were purchased Beyotime Biotechnology (Haimen, China). A PrimeScript RT reagent kit (cat no. RR037A) and a TB Green Fast qPCR Mix kit (cat no. RR430A) were purchased from TaKaRa Biotechnology. Cell Counting Kit-8 (cat no. HY-K0301) was purchased from MedChemExpress (NJ, USA). Phosphatase inhibitors (cat no. C0001) and protease inhibitors (cat no. C0004) were purchased from TargetMol (Boston, MA, USA). All ssDNA were dissolved in sterile water and stored at −20°C. PI3Kγ siRNA were dissolved in DEPC water (cat no. B501005; Sangon, Shanghai, China).

Cell culture

The mouse breast cancer cell line 4T1 and mouse macrophage cell line RAW 264.7 were obtained from the American Type Culture Collection (ATCC; Rockville, MD, USA) and cultured in
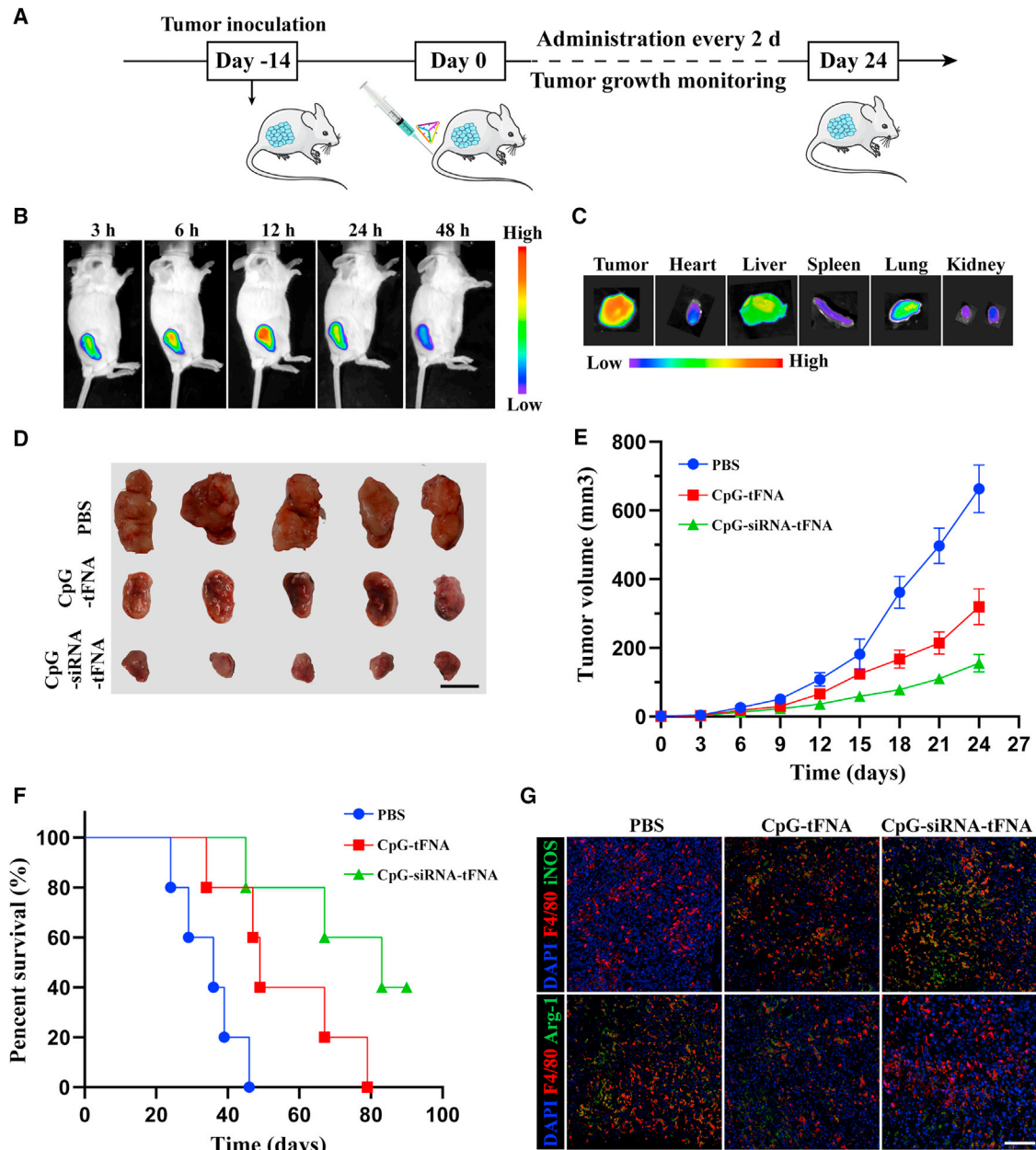
Figure 7. Immunotherapeutic effects of CpG-siRNA-tFNA in 4T1-1-bearing mice

(A) Schedule of CpG-siRNA-tFNA treatment in 4T1-bearing mice. (B) Representative *in vivo* fluorescence imaging. (C) *Ex vivo* fluorescence imaging in major organs. (D) Photographs of the tumor tissue from each group (n = 5, scale bar, 1 cm). (E and F) Tumor growth profiles (E) and survival percentages (F) of mice receiving different treatments (n = 5). (G) Immunofluorescence dual-staining analysis of iNOS and Arg-1 expression of tumor tissue slices at the time point 24 days of treatment scheme (scale bar, 100 μm).

RPMI 1640 medium (cat no. 11,875,168; Gibco, Grand Island, NY, USA), supplemented with 10% fetal bovine serum (cat no. 12,483,020, GIBCO) and 1% penicillin-streptomycin (cat no. C100C5; NCM Biotech, Suzhou, China). All cell lines were incubated in an atmosphere of 5% CO_2 at 37°C according to ATCC guidelines.

Preparation of tFNA, CpG-tFNA, and CpG-RNAi-tFNA

DNA self-assembly structures were prepared as reported previously.[57] Prior to use, all ssDNA at desired concentration were heated for 5 min at 95°C and then cooled to room temperature for 1 h to allow sequences to form energetically favorable secondary structures. For tFNA, six different ssDNA mixtures of component oligonucleotides

(S1, S2, S3, S4, S5, and S6) were combined in TM buffer (10 mM Tris, 5 mM MgCl$_2$), heated to 95°C for 2 min and then rapidly cooled to 4°C for 30 min in a T100 Thermal Cycler (Bio-Rad, Hercules, CA, USA). Each ssDNA strand's final concentration was 1 μM. The CpG-tFNA and CpG-RNAi-tFNA were prepared in the same way.

Gel electrophoresis

Agarose gel electrophoresis was performed to confirm the successful assembly of tFNA, CpG-tFNA, and CpG-RNAi-tFNA. The experiments were operated in 1× TBE running buffer under the condition of 100 V. After nucleic acid stain (4S GelRed, cat no. A616697; Sangon, Shanghai, China) was disposed, the gel was visualized with an imaging system (Bio-Rad).

Stability analysis of tFNA

To test the nanostructures' stability, tFNA and dsDNA were separately incubated with fetal bovine serum of equal volume at 37°C for different time periods (0, 3, 6, 12, and 24 h). The mixtures were then subjected to 2% agarose gel.

Cellular uptake

RAW 264.7 cells were grown on glass coverslips in 24-well culture plates at a density of 5 × 10^5 cells/mL and incubated at 37°C for 24 h. They were then washed with sterile PBS and changed into fresh RPMI 1640. Next, cells were separately incubated with fluorescently labeled 100 nM CpG and CpG-tFNA at 37°C. After being cultured for 1 h, all cells were washed with pre-cold PBS three times and then fixed with 4% formaldehyde (cat. no. P1110; Solarbio, Beijing, China) for 20 min at room temperature, and cell nuclei were treated with DAPI for 10 min. Finally, all confocal images were captured using a laser confocal microscope (Leica TCS SP8, Germany).

Cellular cytotoxicity assays

RAW 264.7 cells were seeded in a 96-well plate with 5 × 10^3 cells per well in 100 μL and cultured for cell adhesion. The medium was replaced with 100 μL of fresh medium containing CpG-tFNA or CpG-RNAi-tFNA at different concentrations. The cells were further incubated for 48 h at 37°C. Then, the medium was replaced with fresh culture medium, and CCK-8 solution was added and incubated for 1 h. The absorbance at 450 nm was measured using a Model 680 microplate reader (Bio-Rad).

Real-time PCR

Total RNA was harvested from RAW 264.7 cells and reverse transcribed into cDNA. Relevant inflammatory cytokine gene (Il-6, Il-12, Tnfa) expressions were determined according to the manufacturer's instructions. The sequences of primers are provided in Table S2. The reactions were performed in a volume of 10 μL using the CFX96 Touch Real-Time PCR Detection System (Bio-Rad).

ELISA assay

RAW 264.7 cells were seeded in a six-well plate and cultured for cell adhesion. Then, the medium was replaced with 2 mL of fresh medium containing different concentrations CpG-tFNA or CpG-RNAi-tFNA for 24 h. The supernatants were collected and the levels of cytokines were determined by an ELISA assay according to the manufacturer's protocol.

Western blotting

Whole protein from RAW 264.7 cells were harvested with RIPA buffer containing proteinase and phosphatase inhibitor cocktail. The protein concentration was measured by BCA assay. Protein samples were separated on SDS-polyacrylamide gels and transferred onto polyvinylidene difluoride (PVDF) membranes. The membranes were blocked with 5% non-fat dry milk in Tris-buffered saline with 0.05% Tween 20 (TBST) for 1 h followed by incubation at 4°C overnight with the primary antibodies. HRP anti-rabbit IgG was used as the secondary antibody. The signals were analyzed using an enhanced chemiluminescence detection system (Bio-Rad).

Transwell assays

RAW 264.7 cells and 4T1 cells were co-cultured using the Transwell system (Millipore, Bedford, MA, USA) with 3-μm pore-size. Then, CpG-tFNA and CpG-RNAi-tFNA were added to the upper chamber. After incubation for 48 h, the cell viability of 4T1 cells in the lower chamber was determined by a CCK-8 assay.

Caspase-3 activity assay

A transwell system (3-μm-pore polycarbonate filter membrane) was used to explore the antitumor effect of CpG-RNAi-tFNA. RAW 264.7 cells and 4T1 cells were respectively added to the upper and lower chambers and cultured in RPMI 1640 containing 10% FBS for 24 h. Then, CpG-tFNA and CpG-RNAi-tFNA were added to the upper chamber. After incubation for 24 h, the 4T1 cells were collected, and the activity of caspase-3 was determined with the caspase-3 activity kit.

Apoptosis assay

4T1 cells were harvested with EDTA-free trypsin and washed with cold PBS three times. Subsequently, the cells were resuspended in 500 μL of PBS and stained with 5 μL of annexin V-fluorescein isothiocyanate (FITC) and 5 μL of propidium iodide (PI) for 15 min in the dark at room temperature. Finally, the apoptosis of 4T1 cells was evaluated by FACScan flow cytometer (BD Biosciences).

Flow cytometry

Briefly, RAW 264.7 cells were treated with CpG-siRNA-tFNA for 24 h. Then, the cells were resuspended in 500 μL of PBS and treated with 1% Triton X-100 solution (cat, no. T8200, Solarbio) for 10 min at room temperature. Next, the cells were blocked with anti-CD16/32 for 10 min at 4°C. After being washed with cold PBS, the cells were incubated with anti-CD86 and anti-CD206 for 30 min in darkness. Finally, the expression of CD86 and CD206 were evaluated by flow cytometry.

Preparation of bone marrow-derived macrophages from BALB/c mice

Bone marrow-derived macrophages were generated as previously described.[58] Femurs and tibias were isolated from mice, and muscle was removed. Then, both ends of the bones were cut with scissors and flushed with RPMI 1640. Cells were cultured in RPMI 1640 containing 10% FBS, 1% penicillin-streptomycin, 2 mM L-glutamine, 50 ng/mL M-CSF (cat, no. 51112-MNAH; Sino Biological, Beijing, China), and experiments were performed after 1 week of culture.

In vivo imaging and therapeutic assay

Female BALB/c mice (5–6 weeks old) were purchased from the Experimental Animal Center of Chongqing Medical University and used following protocols approved by the Ethics Committee of Chongqing Medical University. A total of 1×10^6 4T1 cells were subcutaneously injected into the right flank of each mouse. When the tumors grew to a detectable volume, the mice were intravenously injected in the tail vein with CY7-labeled CpG-siRNA-tFNA (5 mg/kg). Fluorescence images were captured by an *in vivo* imaging system (LB983 NightOWLII, Berthold Technologies) at 3, 6, 12, 24, and 48 h. At 12 h, mice were euthanized, and the fluorescence images of main organs and tumors were performed. The tumor-bearing mice were randomly divided into three groups (5 mice per group). Mice in each group were intravenously injected in the tail vein with PBS, CpG-tFNA, and CpG-siRNA-tFNA (5 mg/kg), respectively, every 3 days. The volumes of tumors were detected by measuring the size of the tumors every 3 days according to the equation: $V = lw^2/2$, (where l and w are the longer and shorter diameters of the tumor).

Immunohistochemistry

After the 4T1-bearing mice were euthanized, tumors were excised and fixed in 4% formaldehyde, embedded in paraffin, and then sliced into 4-μm sections. After deparaffinating and immunostaining with primary and secondary antibodies, the sections were observed with microscopy (Nikon ECLIPSE Ti-s, Japan).

Statistical analysis

Student's t test or one-way ANOVA was used to assess the differences between treated and control groups with GraphPad Prism 8.0.1. All quantitative results are presented as means ± SD (standard deviation) with at least three independent repetitive experiments; $p < 0.05$ was considered to be significant: $^*p < 0.05$, $^{**}p < 0.01$, $^{***}p < 0.01$, $^{****}p < 0.0001$.

SUPPLEMENTAL INFORMATION

Supplemental information can be found online at https://doi.org/10.1016/j.omtn.2021.12.036.

AUTHOR CONTRIBUTIONS

H.Q. and T.Z.: cell experiments, drafting the manuscript, data acquisition, data analysis, and manuscript revision. Y.F., D.Z., M.G., and W.Y.: material and technological support, and data arrangement and analysis. W.F., M.Y., H.S., and C.C.: study concept and supervision; W.C., S.D., and T.C.: manuscript revision, study concept, design, supervision, and funding. All authors read and approved the final manuscript.

DECLARATION OF INTERESTS

The authors declare no competing interests.

REFERENCES

1. Qian, B.-Z., and Pollard, J.W. (2010). Macrophage diversity enhances tumor progression and metastasis. Cell *141*, 39–51.

2. Cassetta, L., and Pollard, J.W. (2020). Tumor-associated macrophages. Curr. Biol. *30*, R246–R248.

3. Chen, Y., Song, Y., Du, W., Gong, L., Chang, H., and Zou, Z. (2019). Tumor-associated macrophages: an accomplice in solid tumor progression. J. Biomed. Sci. *26*, 1–13.

4. Siveen, K., and Kuttan, G. (2009). Role of macrophages in tumour progression. Immunol. Lett. *123*, 97–102.

5. Martinez, F.O., Sica, A., Mantovani, A., and Locati, M. (2008). Macrophage activation and polarization. Front. Biosci. *13*, 453–461.

6. Mantovani, A., and Sica, A. (2010). Macrophages, innate immunity and cancer: balance, tolerance, and diversity. Curr. Opin. Immunol. *22*, 231–237.

7. Liu, Y.-C., Zou, X.-B., Chai, Y.-F., and Yao, Y.-M. (2014). Macrophage polarization in inflammatory diseases. Int. J. Biol. Sci. *10*, 520.

8. Orecchioni, M., Ghosheh, Y., Pramod, A.B., and Ley, K. (2019). Macrophage polarization: different gene signatures in M1 (LPS+) vs. classically and M2 (LPS–) vs. alternatively activated macrophages. Front. Immunol. *10*, 1084.

9. Shu, Y., and Cheng, P. (2020). Targeting tumor-associated macrophages for cancer immunotherapy. Biochim. Biophys. Acta Rev. Cancer *1874*, 188434.

10. Park, J.E., Dutta, B., Tse, S.W., Gupta, N., Tan, C.F., Low, J.K., Yeoh, K.W., Kon, O.L., Tam, J.P., and Sze, S.K. (2019). Hypoxia-induced tumor exosomes promote M2-like macrophage polarization of infiltrating myeloid cells and microRNA-mediated metabolic shift. Oncogene *38*, 5158–5173.

11. Jing, X., Yang, F., Shao, C., Wei, K., Xie, M., Shen, H., and Shu, Y. (2019). Role of hypoxia in cancer therapy by regulating the tumor microenvironment. Mol. Cancer *18*, 157.

12. He, Y., Cong, C., He, Y., Hao, Z., Li, C., Wang, S., Zhao, Q., He, H., Zhu, R., and Li, X. (2019). Tumor hypoxia relief overcomes multidrug resistance and immune inhibition for self-enhanced photodynamic therapy. Chem. Eng. J. *375*, 122079.

13. Heusinkveld, M., and van der Burg, S.H. (2011). Identification and manipulation of tumor associated macrophages in human cancers. J. Transl. Med. *9*, 216.

14. Lissbrant, I.F., Stattin, P., Wikstrom, P., Damber, J., Egevad, L., and Bergh, A. (2000). Tumor associated macrophages in human prostate cancer: relation to clinicopathological variables and survival. Int. J. Oncol. *17*, 445–496.

15. Zhang, B.C., Gao, J., Wang, J., Rao, Z.G., Wang, B.C., and Gao, J.F. (2011). Tumor-associated macrophages infiltration is associated with peritumoral lymphangiogenesis and poor prognosis in lung adenocarcinoma. Med. Oncol. *28*, 1447–1452.

16. Xu, X., Gong, X., Wang, Y., Li, J., Wang, H., Wang, J., Sha, X., Li, Y., and Zhang, Z. (2020). Reprogramming tumor associated macrophages toward M1 phenotypes with nanomedicine for anticancer immunotherapy. Adv. Ther. *3*, 1900181.

17. Zang, X., Zhang, X., Zhao, X., Hu, H., Qiao, M., Deng, Y., and Chen, D. (2019). Targeted delivery of miRNA 155 to tumor associated macrophages for tumor immunotherapy. Mol. Pharm. *16*, 1714–1722.

18. Merlano, M., Abbona, A., Denaro, N., and Garrone, O. (2019). Knowing the tumour microenvironment to optimise immunotherapy. Acta Otorhinolaryngol. Ital. *39*, 2.

19. Nie, W., Wu, G., Zhang, J., Huang, L.L., Ding, J., Jiang, A., Zhang, Y., Liu, Y., Li, J., and Pu, K. (2020). Responsive exosome nano-bioconjugates for synergistic cancer therapy. Angew. Chem. 132, 2034–2038.

20. Yu, M., Duan, X., Cai, Y., Zhang, F., Jiang, S., Han, S., Shen, J., and Shuai, X. (2019). Multifunctional nanoregulator reshapes immune microenvironment and enhances immune memory for tumor immunotherapy. Adv. Sci. 6, 1900037.

21. Cai, H., Shukla, S., and Steinmetz, N.F. (2020). The antitumor efficacy of CpG oligonucleotides is improved by encapsulation in plant virus-like particles. Adv. Funct. Mater. 30, 1908743.

22. Reynolds, A., Leake, D., Boese, Q., Scaringe, S., Marshall, W.S., and Khvorova, A. (2004). Rational siRNA design for RNA interference. Nat. Biotechnol. 22, 326–330.

23. Hu, B., Zhong, L., Weng, Y., Peng, L., Huang, Y., Zhao, Y., and Liang, X.-J. (2020). Therapeutic siRNA: state of the art. Signal. Transduct. Target. Therapy 5, 1–25.

24. Xia, H., Mao, Q., Paulson, H.L., and Davidson, B.L. (2002). siRNA-mediated gene silencing in vitro and in vivo. Nat. Biotechnol. 20, 1006–1010.

25. Gavrilov, K., and Saltzman, W.M. (2012). Therapeutic siRNA: principles, challenges, and strategies. Yale J. Biol. Med. 85, 187.

26. Wang, T., Shigdar, S., Al Shamaileh, H., Gantier, M.P., Yin, W., Xiang, D., Wang, L., Zhou, S.-F., Hou, Y., and Wang, P. (2017). Challenges and opportunities for siRNA-based cancer treatment. Cancer Lett. 387, 77–83.

27. Ge, Z., Gu, H., Li, Q., and Fan, C. (2018). Concept and development of framework nucleic acids. J. Am. Chem. Soc. 140, 17808–17819.

28. Zhang, T., Cui, W., Tian, T., Shi, S., and Lin, Y. (2020). Progress in biomedical applications of tetrahedral framework nucleic acid-based functional systems. ACS Appl. Mater. Inter. 12, 47115–47126.

29. Xue, H., Ding, F., Zhang, J., Guo, Y., Gao, X., Feng, J., Zhu, X., and Zhang, C. (2019). DNA tetrahedron-based nanogels for siRNA delivery and gene silencing. Chem. Commun. 55, 4222–4225.

30. Liu, J., Song, L., Liu, S., Zhao, S., Jiang, Q., and Ding, B. (2018). A tailored DNA nanoplatform for synergistic RNAi-/chemotherapy of multidrug-resistant tumors. Angew. Chem. Int. Ed. Engl. 57, 15486–15490.

31. Ruan, W., Zheng, M., An, Y., Liu, Y., Lovejoy, D.B., Hao, M., Zou, Y., Lee, A., Yang, S., Lu, Y., et al. (2018). DNA nanoclew templated spherical nucleic acids for siRNA delivery. Chem. Commun. 54, 3609–3612.

32. Bujold, K.E., Hsu, J.C.C., and Sleiman, H.F. (2016). Optimized DNA "nanosuitcases" for encapsulation and conditional release of siRNA. J. Am. Chem. Soc. 138, 14030–14038.

33. Bode, C., Zhao, G., Steinhagen, F., Kinjo, T., and Klinman, D.M. (2011). CpG DNA as a vaccine adjuvant. Expert Rev. Vaccin. 10, 499–511.

34. Vollmer, J. (2006). CpG motifs to modulate innate and adaptive immune responses. Int. Rev. Immunol. 25, 125–134.

35. Krieg, A.M. (2008). Toll-like receptor 9 (TLR9) agonists in the treatment of cancer. Oncogene 27, 161–167.

36. Nechaev, S., Gao, C., Moreira, D., Swiderski, P., Jozwiak, A., Kowolik, C.M., Zhou, J., Armstrong, B., Raubitschek, A., and Rossi, J.J. (2013). Intracellular processing of immunostimulatory CpG–siRNA: toll-like receptor 9 facilitates siRNA dicing and endosomal escape. J. Control Release 170, 307–315.

37. Kortylewski, M., Swiderski, P., Herrmann, A., Wang, L., Kowolik, C., Kujawski, M., Lee, H., Scuto, A., Liu, Y., and Yang, C. (2009). In vivo delivery of siRNA to immune cells by conjugation to a TLR9 agonist enhances antitumor immune responses. Nat. Biotechnol. 27, 925–932.

38. Kaneda, M.M., Messer, K.S., Ralainirina, N., Li, H., Leem, C.J., Gorjestani, S., Woo, G., Nguyen, A.V., Figueiredo, C.C., and Foubert, P. (2016). PI3Kγ is a molecular switch that controls immune suppression. Nature 539, 437–442.

39. De Henau, O., Rausch, M., Winkler, D., Campesato, L.F., Liu, C., Cymerman, D.H., Budhu, S., Ghosh, A., Pink, M., and Tchaicha, J. (2016). Overcoming resistance to checkpoint blockade therapy by targeting PI3Kγ in myeloid cells. Nature 539, 443–447.

40. Lee, Y.S., Song, S.J., Hong, H.K., Oh, B.Y., Lee, W.Y., and Cho, Y.B. (2020). The FBW7-MCL-1 axis is key in M1 and M2 macrophage-related colon cancer cell progression: validating the immunotherapeutic value of targeting PI3Kγ. Exp. Mol. Med. 52, 1–17.

41. Luo, L., Wall, A.A., Tong, S.J., Hung, Y., Xiao, Z., Tarique, A.A., Sly, P.D., Fantino, E., Marzolo, M.-P., and Stow, J.L. (2018). TLR crosstalk activates LRP1 to recruit Rab8a and PI3Kγ for suppression of inflammatory responses. Cell Rep. 24, 3033–3044.

42. Wall, A.A., Luo, L., Hung, Y., Tong, S.J., Condon, N.D., Blumenthal, A., Sweet, M.J., and Stow, J.L. (2017). Small GTPase Rab8a-recruited phosphatidylinositol 3-kinase γ regulates signaling and cytokine outputs from endosomal toll-like receptors. J. Biol. Chem. 292, 4411–4422.

43. Xie, N., Huang, J., Yang, X., Yang, Y., Quan, K., Wang, H., Ying, L., Ou, M., and Wang, K. (2016). A DNA tetrahedron-based molecular beacon for tumor-related mRNA detection in living cells. Chem. Commun. 52, 2346–2349.

44. Biswas, S.K., and Lewis, C.E. (2010). NF-κB as a central regulator of macrophage function in tumors. J. Leukoc. Biol. 88, 877–884.

45. He, X.-Y., Liu, B.-Y., Wu, J.-L., Ai, S.-L., Zhuo, R.-X., and Cheng, S.-X. (2017). A dual macrophage targeting nanovector for delivery of oligodeoxynucleotides to overcome cancer-associated immunosuppression. ACS Appl. Mater. Inter. 9, 42566.

46. Klinman, D.M. (2004). Immunotherapeutic uses of CpG oligodeoxynucleotides. Nat. Rev. Immunol. 4, 249–259.

47. Chen, Q., Wang, C., Zhang, X., Chen, G., Hu, Q., Li, H., Wang, J., Wen, D., Zhang, Y., and Lu, Y. (2019). In situ sprayed bioresponsive immunotherapeutic gel for post-surgical cancer treatment. Nat. Nanotechnol. 14, 89–97.

48. Zanganeh, S., Hutter, G., Spitler, R., Lenkov, O., Mahmoudi, M., Shaw, A., Pajarinen, J.S., Nejadnik, H., Goodman, S., and Moseley, M. (2016). Iron oxide nanoparticles inhibit tumour growth by inducing pro-inflammatory macrophage polarization in tumour tissues. Nat. Nanotechnol. 11, 986–994.

49. Wang, C., Yu, Y., Irfan, M., Xu, B., Li, J., Zhang, L., Qin, Z., Yu, C., Liu, H., and Su, X. (2020). Rational design of DNA framework-based hybrid nanomaterials for anti-cancer drug delivery. Small 16, 2002578.

50. Zhao, H., Lv, J., Li, F., Zhang, Z., Zhang, C., Gu, Z., and Yang, D. (2021). Enzymatical biomineralization of DNA nanoflowers mediated by manganese ions for tumor site activated magnetic resonance imaging. Biomaterials 268, 120591.

51. Chen, Y., Hong, T., Wang, S., Mo, J., Tian, T., and Zhou, X. (2017). Epigenetic modification of nucleic acids: from basic studies to medical applications. Chem. Soc. Rev. 46, 2844–2872.

52. Micklefield, J. (2001). Backbone modification of nucleic acids: synthesis, structure and therapeutic applications. Curr. Med. Chem. 8, 1157–1179.

53. Ni, S., Zhuo, Z., Pan, Y., Yu, Y., Li, F., Liu, J., Wang, L., Wu, X., Li, D., and Wan, Y. (2020). Recent progress in aptamer discoveries and modifications for therapeutic applications. ACS Appl. Mater. Inter. 13, 9500–9519.

54. Buntz, A., Killian, T., Schmid, D., Seul, H., Brinkmann, U., Ravn, J., Lindholm, M., Knoetgen, H., Haucke, V., and Mundigl, O. (2019). Quantitative fluorescence imaging determines the absolute number of locked nucleic acid oligonucleotides needed for suppression of target gene expression. Nucleic Acids Res. 47, 953–969.

55. Hagedorn, P.H., Persson, R., Funder, E.D., Albæk, N., Diemer, S.L., Hansen, D.J., Møller, M.R., Papargyri, N., Christiansen, H., and Hansen, B.R. (2018). Locked nucleic acid: modality, diversity, and drug discovery. Drug Discov. Today 23, 101–114.

56. Li, X., Li, Z., and Yu, H. (2020). Selection of threose nucleic acid aptamers to block PD-1/PD-L1 interaction for cancer immunotherapy. Chem. Commun. 56, 14653–14656.

57. Lee, H., Lytton-Jean, A.K., Chen, Y., Love, K.T., Park, A.I., Karagiannis, E.D., Sehgal, A., Querbes, W., Zurenko, C.S., and Jayaraman, M. (2012). Molecularly self-assembled nucleic acid nanoparticles for targeted in vivo siRNA delivery. Nat. Nanotechnol. 7, 389–393.

58. Anzinger, J.J., Chang, J., Xu, Q., Barthwal, M.K., Bohnacker, T., Wymann, M.P., and Kruth, H.S. (2012). Murine bone marrow-derived macrophages differentiated with GM-CSF become foam cells by PI3Kγ-dependent fluid-phase pinocytosis of native LDL [S]. J. Lipid Res. 53, 34–42.